Spatial force correlations in granular shear flow. II. Theoretical implications

Gregg Lois,[1] Anaël Lemaître,[2] and Jean M. Carlson[1]
[1]*Department of Physics, University of California, Santa Barbara, California 93106, USA*
[2]*Institut Navier–LMSGC, 2 allée Képler, 77420 Champs-sur-Marne, France*
(Received 16 December 2006; revised manuscript received 18 April 2007; published 3 August 2007)

Numerical simulations are used to test the kinetic theory constitutive relations of inertial granular shear flow. These predictions are shown to be accurate in the dilute regime, where only binary collisions are relevant, but underestimate the measured value in the dense regime, where force networks of size ξ are present. The discrepancy in the dense regime is due to non-collisional forces that we measure directly in our simulations and arise from elastic deformations of the force networks. We model the non-collisional stress by summing over all paths that elastic waves travel through force networks. This results in an analytical theory that successfully predicts the stress tensor over the entire inertial regime without any adjustable parameters.

DOI: 10.1103/PhysRevE.76.021303 PACS number(s): 81.05.Rm

I. INTRODUCTION

Granular materials exhibit a broad spectrum of behaviors that have been difficult to capture theoretically, especially in the dense regime. A fundamental question is whether, and when, collective motion becomes important for understanding the macroscopic state of the system [1]. This is a particularly complex issue for granular flows, where the material structure remains amorphous on all scales. While a noticeable structural change would surely help pinpoint degrees of freedom that govern collective dynamics, granular flows require us to use the dynamics to search for structure.

A central tool in this process is numerical simulation, and new insights from simulations can provide important clues for theory. In the companion paper [2] we have presented evidence for a length scale that increases with packing fraction and is related to correlations between grain forces. These correlations arise from force chain networks that span the space between grains and transmit forces elastically. By measuring two-point spatial force correlations in steady-state shear flow, we were able to extract a length scale ξ that characterizes the exponential decay of correlations and the effective size of force networks. It was also shown that the mechanisms of momentum transfer are closely related to the presence of force networks and contact force statistics are highly dependent on ξ.

Since contact forces are sensitive to the value of ξ, the derivation of constitutive relations to describe the stress tensor must be based on properties of force networks. While network properties have been incorporated into previous studies of static granular packings [3–9], the importance of force networks in granular flows has not been adequately explored. Instead, constitutive relations are generally obtained using comparisons with liquids [10,11] and especially kinetic theory [12–14], which can be extended to treat dense materials [15–17] as long as correlations beyond nearest neighbors are absent.

In this paper we examine two models for constitutive relations in granular flow: kinetic theory and a model referred to as the force network model. Kinetic theory is rooted in the dilute limit and assumes no spatial correlations between grains. The force network model is motivated by our simulations and attempts to capture the effects of finite-sized force networks in a mean-field framework, which spans system behavior from dilute to dense regimes.

The predictions of these models are compared using measurements of the stress tensor $\Sigma_{\alpha\beta}$, which is given by

$$\Sigma_{\alpha\beta}V = \sum_{i=1}^{N} m^i (v_\alpha^i - u_\alpha)(v_\beta^i - u_\beta) + \sum_{\{i,j\}=1}^{c} \boldsymbol{\sigma}_\alpha^{ij} \mathbf{F}_\beta^{ij}. \quad (1)$$

In this equation, Greek subscripts denote components, italic superscripts denote grains, and V represents the volume. The first term quantifies stress resulting from fluctuating velocities, which is related to the mass of each grain, m^i, and the difference between grain velocity $\mathbf{v}^i$ and average velocity $\mathbf{u}$ (where boldface symbols denote full, three-component vectors). The second term arises from contacts between grains: it depends on the contact forces $\mathbf{F}^{ij}$ and the distance between contacting grains, $\boldsymbol{\sigma}^{ij}$. The sum is taken over all contacts $\{i,j\}$ in the system.

We focus here on the second term, which is directly associated with contact forces and historically called the static stress, and specialize on nonfrictional systems where $\boldsymbol{\sigma}^{ij} \times \mathbf{F}^{ij} = 0$. This allows us to write the static stress tensor $\Sigma^{\mathrm{s}}_{\alpha\beta}$ as

$$\Sigma^{\mathrm{s}}_{\alpha\beta}V = \sum_{\{i,j\}=1}^{c} \hat{\sigma}_\alpha^{ij} \hat{\sigma}_\beta^{ij} \sigma^{ij} F^{ij}, \quad (2)$$

where $\boldsymbol{\sigma}^{ij} = \sigma^{ij}\hat{\boldsymbol{\sigma}}^{ij}$ and F^{ij} is the magnitude of the contact force between pairs $\{i,j\}$ of contacting grains. In what follows we will further separate the static stress into a "collisional" component, arising from instantaneous binary collisions between grains, and an "elastic" component, arising from long-lasting contact forces between grains in force networks. This makes a total of three contributions to the stress tensor: a kinetic term due to fluctuating velocities (which is small and we ignore here), a collisional term that we demonstrate is well described by kinetic theory, and an elastic term that precipitates the breakdown of kinetic theory in the dense inertial regime. All measurements are made using two-dimensional contact dynamics (CD) simulations of simple shear flow, with parameters identical to those described in

the companion paper [2]. The CD algorithm simulates granular materials in the limit where grains are perfectly rigid. We employ Lees-Edwards boundary conditions to simulate shear at constant volume, without boundary effects.

We begin in Sec. II with an investigation of dilute inertial flows and test the predictions of hard-sphere kinetic theory. We find that kinetic theory begins to break down when elastic stresses become nonzero. In Sec. III we focus on dense inertial flows where this breakdown occurs and introduce the force network model to predict the elastic stresses.

II. DILUTE INERTIAL FLOWS

Over the past 25 years [18,19] the kinetic theory of dense gases has been generalized to include granular flows, where thermal fluctuations are absent and energy is dissipated at each contact. The dissipation mechanism most often considered is instantaneous collisions with constant restitution coefficient—this is called hard-sphere kinetic theory [20]. In order to make progress using hard-sphere kinetic theory, it is necessary to *begin* by postulating that only binary collisions occur between grains. Without this assumption, calculations quickly become intractable since high-order correlations must be included in kinetic integrals.

The principal microscopic input to hard-sphere kinetic theory is the collision rule between grains. This relates the initial velocities of two interacting grains $\{\mathbf{v}'^i,\mathbf{v}'^j\}$ to their final velocities $\{\mathbf{v}^i,\mathbf{v}^j\}$:

$$(\mathbf{v}^j-\mathbf{v}^i)\cdot\hat{\boldsymbol{\sigma}}^{ij}=-e(\mathbf{v}'^j-\mathbf{v}'^i)\cdot\hat{\boldsymbol{\sigma}}^{ij}. \tag{3}$$

The normal coefficient of restitution e that appears in this equation determines the energy dissipated in each collision: for $e=1$ the system is elastic and no energy is dissipated; as e is reduced to zero, the energy dissipation scales as $1-e^2$.

Kinetic theory relies on the assumption that only binary collision are relevant and is therefore expected to break down as the density of the flow increases and long-lasting contacts arise [21–24]. Quantitative bounds over which the binary collision assumption holds have only recently been estimated [25,26]. The CD algorithm used here to simulate granular flows is well suited for testing the relevance of the binary collision assumption and bounding the dilute regime. Like hard-sphere kinetic theory, the CD algorithm employs a normal coefficient of restitution. However the CD algorithm does not assume *a priori* that only binary collisions occur.

On the contrary, we observe that multigrain contacts are the dominant interaction in dense flows. This is evident in force correlation measurements [2], which identify a growing correlation length ξ. This length scale should be an indicator of the breakdown of the binary collision assumption since it implies that grain forces are correlated over large distances and do not simply depend on nearest neighbors. To see how this comes about, it is useful to measure the static stress tensor.

Equation (2) gives the microscopic expression for the static stress tensor, which depends on contact forces between grains. In the case that only binary collisions are considered, as in kinetic theory, the value of the static stress tensor is determined by inserting the binary collisional force into Eq. (2). The collisional force is the force that occurs between a pair of colliding grains that are not part of a force network. Given the initial velocities $\mathbf{v}'^i$ of grains i, the collisional force between two grains is given by

$$F_{\mathrm{bc}}^{ij}=(1+e)\mu^{ij}[(\mathbf{v}'^j-\mathbf{v}'^i)\cdot\hat{\boldsymbol{\sigma}}^{ij}]/dt, \tag{4}$$

where e is the normal restitution coefficient, $\mu=m^im^j/(m^i+m^j)$ is the reduced mass, and $\hat{\boldsymbol{\sigma}}^{ij}$ is the unit vector connecting the centers of grains i and j. This expression is equal to the change of momentum of grains i and j, per simulation time step dt, due to binary interactions. Since all of the parameters can be measured in simulations, the collisional force is a useful probe of the dynamics and was used in the companion paper to exhibit the presence of force networks.

Inserting the collisional force into Eq. (2) yields the "collisional" stress tensor

$$\Sigma_{\alpha\beta}^{\mathrm{bc}}=\sum_{\{i,j\}=0}^{c}\hat{\sigma}_\alpha^{ij}\hat{\sigma}_\beta^{ij}\sigma^{ij}F_{\mathrm{bc}}^{ij}, \tag{5}$$

which only includes the effects of binary collisions between grains and is the stress tensor that all hard-sphere kinetic theories attempt to model [26]. This is because only binary collisions between grains are considered and contact forces can be no larger than the value given in Eq. (4).

If relevant interactions occur only via binary collisions, the collisional stress in Eq. (5) and the static stress in Eq. (2) are identical. However, a discrepancy between the collisional and static stress tensors indicates that momentum transfer is not carried out by binary collisions alone. Comparing the static and collisional stress tensors in Eqs. (2) and (5) therefore provides an opportunity to test the binary collision assumption and thereby determine when kinetic theory can be applied to hard-sphere granular flows.

In Figs. 1 and 2 we plot measurements of the static and collisional stress tensor for a wide range of restitution coefficients and packing fractions in terms of the pressure p and shear stress s, which are related to the stress tensors by

$$\{p^{\mathrm{s}},p^{\mathrm{bc}}\}=\left\{\frac{1}{2}(\Sigma_{11}^{\mathrm{s}}+\Sigma_{22}^{\mathrm{s}}),\frac{1}{2}(\Sigma_{11}^{\mathrm{bc}}+\Sigma_{22}^{\mathrm{bc}})\right\}, \tag{6}$$

$$\{s^{\mathrm{s}},s^{\mathrm{bc}}\}=\{\Sigma_{12}^{\mathrm{s}},\Sigma_{12}^{\mathrm{bc}}\}=\{\Sigma_{21}^{\mathrm{s}},\Sigma_{21}^{\mathrm{bc}}\}. \tag{7}$$

In Figs. 1 and 2 both the collisional and static values of the pressure and shear stress are normalized by common factors that are explained later, in the paragraph beneath Eq. (14). For now, it is only important to note that there is a dilute regime where the binary collision assumption holds and the collisional and static stress tensors are equal. The bounds of this regime depend on the value of both the restitution coefficient and the packing fraction. The data support a conclusion that the dilute regime is approached as the density is reduced or restitution is increased. For high densities the collisional and static stress are not equal, and there is a nonzero elastic component of stress. The data support the existence of both a dilute regime, where only binary collisions are relevant, and a dense regime, where elastic stresses become important.

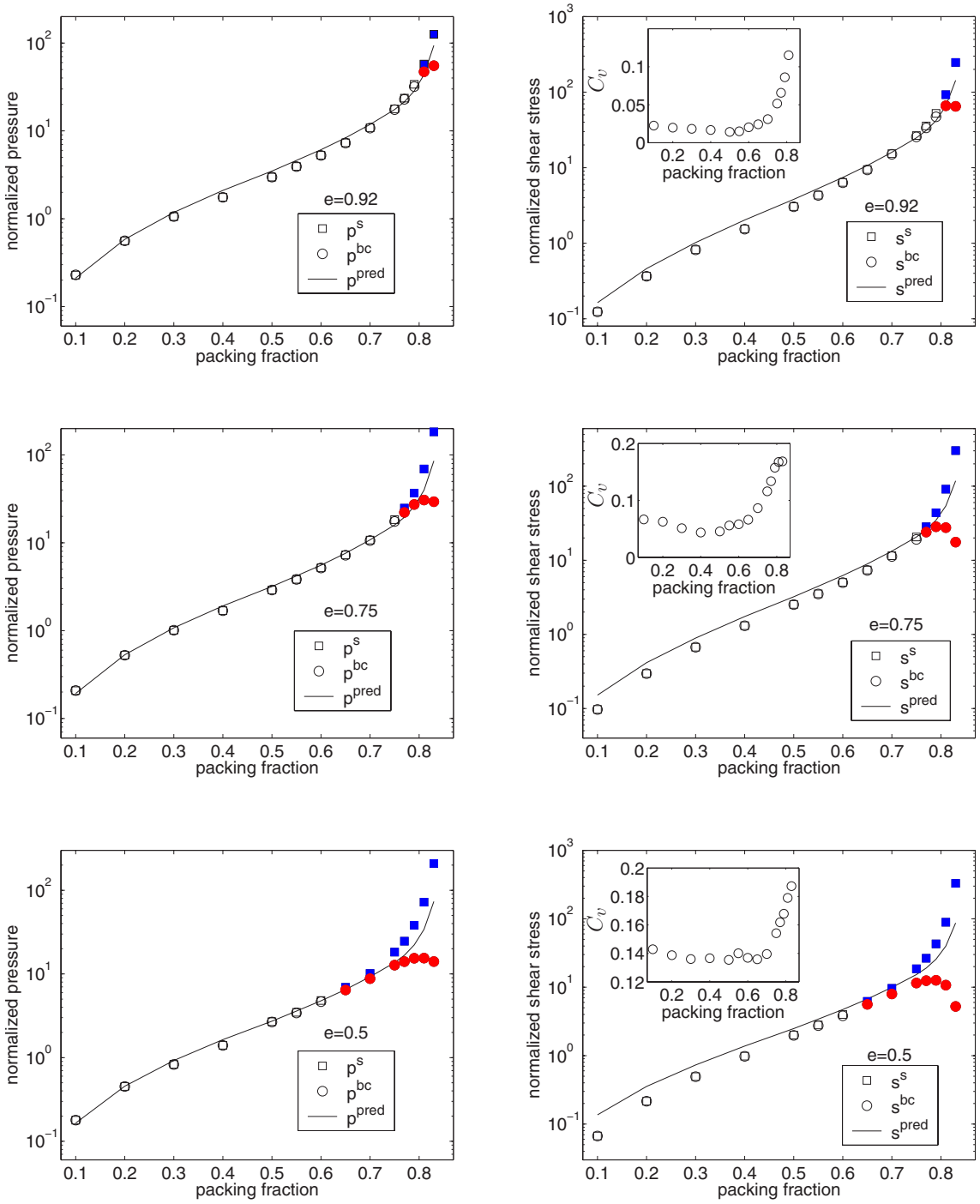

FIG. 1. (Color online) Main figures: normalized values of the pressure (left) and shear stress (right) for large restitution coefficients $e=0.92$, $e=0.75$, and $e=0.5$. The pressure is normalized by p_0 from Eq. (12) and the shear stress is normalized by $\dot{\gamma}\eta_0$ from Eq. (13) . The dilute regime is characterized by the range of restitution and packing where the static and collisional values are equal. Solid data points correspond to values of restitution and packing where $\xi/\xi_{\mathrm{el}}>1.25$—this provides a simple quantitative condition for the boundary of the dilute regime. Kinetic theory is expected to apply in the dilute regime, and the prediction for the pressure is accurate for all e. The prediction for the shear stress overestimates the actual value, due to positive velocity correlations. Insets: precollisional velocity correlations as a function of packing fraction [defined in Eq. (15)].

In the companion paper [2] it was shown that the there is a well-defined transition between dilute and dense regimes that occurs at the empirically determined value of $\xi/\xi_{\mathrm{el}}=1.25$, where ξ is the size of the force networks and ξ_{el} is the size in the limit of low density. This transition takes place when noncollisional elastic forces become relevant to macroscopic observables, and the critical value of ξ can be determined by a qualitative transformation in the contact force statistics. If $\xi/\xi_{\mathrm{el}}=1.25$ is a well-defined transition point, then it should also be relevant in the dilute to dense transfor-

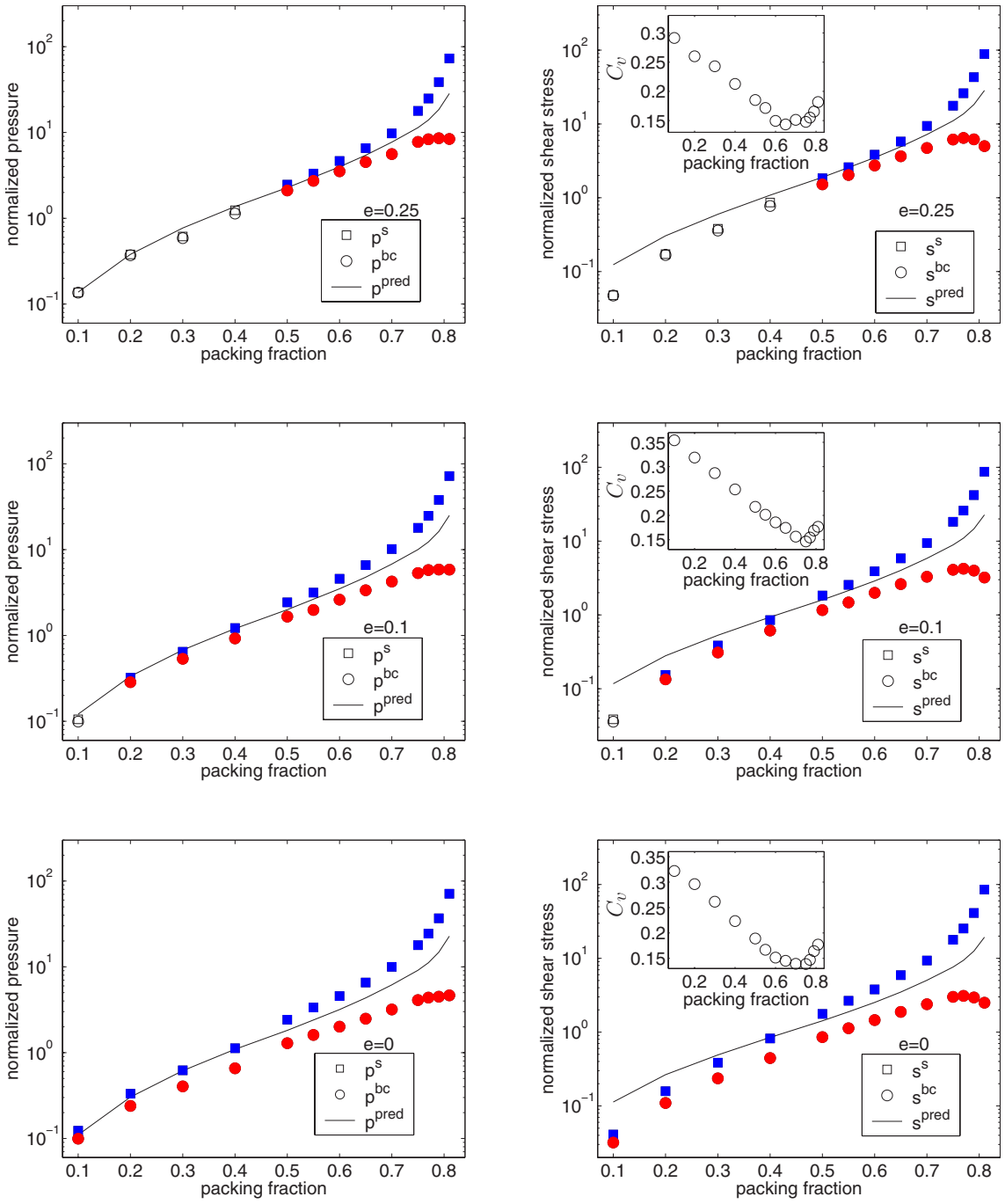

FIG. 2. (Color online) The same as Fig. 1 for small restitution coefficients of $e=0.25$, $e=0.1$, and $e=0$.

mation seen here in the data of the pressure and shear stress. In Figs. 1 and 2 we have colored the data points where $\xi/\xi_{el}>1.25$, using data from the companion paper. For all restitution coefficients, this simple condition on ξ nicely characterizes the dilute regime—if $\xi/\xi_{el}<1.25$, then the static stress tensor is approximately equal to the collisional stress tensor and the predictions of kinetic theory apply; if $\xi/\xi_{el}>1.25$, then interactions between networks of grains become important, the static stress is larger than the collisional stress, and kinetic theory does not apply. This provides further evidence that $\xi/\xi_{el}=1.25$ is a useful quantitative bound for the dilute regime.

In the dilute regime where $\xi/\xi_{el}<1.25$ and $\Sigma^s_{\alpha\beta}=\Sigma^{bc}_{\alpha\beta}$, we can test the predictions of hard-sphere kinetic theory for both the pressure and shear stress. These predictions have been obtained recently [15–17] using the Chapman-Enskog expansion to solve the Enskog equation. The Enskog equation determines the time dependence of the one-particle probability distribution function (PDF) in terms of collision events between grains. Collision events consist of binary interactions and the time dependence of the one-particle PDF can therefore be expressed in terms of just the two-particle PDF. For hard-sphere granular materials, Enskog's equation reads

$$(\partial_t + \mathbf{v}_1 \cdot \boldsymbol{\nabla}_1) f^{(1)}(\mathbf{r}_1, \mathbf{v}_1, t) = J_E[\mathbf{r}_1, \mathbf{v}_1], \tag{8}$$

with J_E given by

$$J_E[\mathbf{r}_1, \mathbf{v}_1] = \sigma \int d\mathbf{v}_2 \int d\hat{\boldsymbol{\sigma}}\, \Theta(\hat{\boldsymbol{\sigma}} \cdot \mathbf{g})(\hat{\boldsymbol{\sigma}} \cdot \mathbf{g})[e^{-2} f^{(2)}(\mathbf{r}_1, \mathbf{r}_1 - \boldsymbol{\sigma}, \mathbf{v}_1', \mathbf{v}_2', t) - f^{(2)}(\mathbf{r}_1, \mathbf{r}_1 + \boldsymbol{\sigma}, \mathbf{v}_1, \mathbf{v}_2, t)]. \tag{9}$$

Physically, the time dependence of the one-particle PDF $f^{(1)}$ is related to a collisional term J_E that quantifies the probability to gain and lose contributions at a certain velocity $\mathbf{v}_1$. The first term in J_E gives the probability that a binary collision between grains results in a grain having velocity $\mathbf{v}_1$, and the second term gives the probability that a binary collision occurs involving a grain that has velocity $\mathbf{v}_1$, thereby reducing $f^{(1)}(\mathbf{v}_1)$. The binary collisions occur according to Eq. (3) and primed velocities represent precollisional values. Θ is the step function and $\mathbf{g}=\mathbf{v}_1-\mathbf{v}_2$. For hard-sphere granular flows, this form for the Enskog equation can be formally derived, starting with the binary collision assumption and the pseudo-Liouville equation [20,27].

A prediction for the collisional stress tensor is obtained by multiplying Eq. (8) on each side by $m\mathbf{v}_1$, where m is the particle mass, and integrating over $\mathbf{v}_1$. This yields the transport equation for momentum density [15], which gives the stress tensor

$$\Sigma_{\alpha\beta}^{\text{pred}} = \frac{1+e}{4} m\sigma \int d\mathbf{v}_1 \int d\mathbf{v}_2 \int d\hat{\boldsymbol{\sigma}}\, \Theta(\hat{\boldsymbol{\sigma}} \cdot \mathbf{g}) \times (\hat{\boldsymbol{\sigma}} \cdot \mathbf{g})^2 \sigma_\alpha \sigma_\beta \int_0^1 d\lambda\, f^{(2)}[\mathbf{r} - (1-\lambda)\boldsymbol{\sigma}, \mathbf{r} + \lambda\boldsymbol{\sigma}, \mathbf{v}_1, \mathbf{v}_2, t]. \tag{10}$$

In order to determine the stress tensor and solve the Enskog equation, it is necessary to express $f^{(2)}$ in terms of $f^{(1)}$. Assuming there are no velocity correlations between grains that are about to collide yields

$$f^{[2]}(\mathbf{r}_1, \mathbf{r}_2, \mathbf{v}_1, \mathbf{v}_2, t) = \chi(\mathbf{r}_1, \mathbf{r}_2) f(\mathbf{r}_1, \mathbf{v}_1, t) f(\mathbf{r}_2, \mathbf{v}_2, t) \tag{11}$$

and reduces the Enskog equation (8) to a nonlinear differential equation for the one-particle PDF. The function χ is interpreted as the equilibrium correlation function at contact and depends on the local value of the density.

Once the Enskog equation has been expressed in terms of only the one-particle PDF, it can be solved using the Chapman-Enskog expansion [28,29], which expands $f^{(1)}$ and J_E in gradients of the mass density, momentum density, and energy density. This process has been carried out for granular shear flows to first order in the gradients in Refs. [15–17]. In two dimensions, this gives predictions [17] for the pressure p^{pred} and shear stress s^{pred}:

$$\frac{p^{\text{pred}}}{p_0} = (1+e)\chi\nu, \tag{12}$$

$$\frac{s^{\text{pred}}}{\dot{\gamma}\eta_0} = \frac{4\nu}{\pi}\left(\frac{4}{5-e} + \nu\chi(1+e)f(e)\right), \tag{13}$$

$$f(e) = \frac{3e-1}{5-e} + \left(1 - \frac{(1-e)(1-2e^2)}{81-17e+30e^2(1-e)}\right), \tag{14}$$

which only depend on the restitution e, the packing fraction ν, and the pair correlation function at contact χ. The normalizing factors are given by $p_0=nmT/2$ and $\eta_0=m/\sigma\sqrt{T/2\pi}$, where m is the grain mass, σ the grain diameter, T the granular temperature, and n the number density. We measure all the variables of Eqs. (12) and (13) in simulations and test the predictions of hard-sphere kinetic theory without fitting parameters. We use the average value of grain mass and diameter for m and σ, and determine χ by tracking the number of collisions that occur per second (which we denote by ω) in equilibrium simulations where $e=1$ and $\dot{\gamma}=0$. Enskog theory relates χ to ω through the equation $\omega=\sqrt{2\pi\delta T}\chi n\sigma$. This method for measuring χ has been used in other recent studies [30].

We plot the normalized predictions from Eqs. (12)–(14) in Figs. 1 and 2, where they are compared to data for the stress tensor. Since hard-sphere kinetic theory assumes binary collisions, the predictions only apply to the dilute regime where $\xi/\xi_{\text{el}} < 1.25$. These are the open symbols in Figs. 1 and 2. We immediately notice that the prediction for the pressure matches the measured pressure in all of the dilute systems we have investigated. Considering that there are no adjustable parameters, this is a tremendous success for kinetic theory.

The prediction for the shear stress matches the data in the dilute regime only for large restitution. As the restitution becomes smaller, the prediction for the shear stress begins to overestimate its measured value. This overestimation is due to precollisional velocity correlations, a mechanism that has been investigated in previous studies [31]. Since Eq. (11) assumes no precollisional velocity correlations, if these correlations exist, then the average momentum transferred in each collision changes. If the precollisional normal velocities of two grains tend to be aligned (antialigned), then the average momentum transferred decreases (increases), causing the kinetic theory prediction to overestimate (underestimate) the measured values.

In the insets of Figs. 1 and 2, we plot measurements of the precollisional velocity correlations C_v defined as

$$C_v = \langle (\mathbf{v}'^i \cdot \hat{\boldsymbol{\sigma}}^{ij})(\mathbf{v}'^j \cdot \hat{\boldsymbol{\sigma}}^{ij}) \rangle / T, \tag{15}$$

which are normalized by the granular temperature. This definition yields a positive value when precollisional grain velocities tend to be aligned, and for all restitution coefficients we observe that the correlations are positive. In addition, the magnitude of the discrepancy between measured and predicted shear stress is roughly proportional to the size of the velocity correlations. These observations support the conclusion that the errors in the kinetic theory prediction are due to precollisional velocity correlations.

To summarize, the stress tensor predicted by hard-sphere kinetic theory matches data from our simulations in the dilute regime where $\xi/\xi_{\text{el}} < 1.25$ and at high restitution coefficients. As the restitution coefficient is decreased in dilute flows, the prediction for the shear stress begins to fail due to the "molecular chaos" assumption of Eq. (11). Additionally, as ξ/ξ_{el} becomes larger than 1.25 in the dense regime, the

hard-sphere kinetic theory predictions are inaccurate since the binary collision assumption is not valid. These observations indicate that the fundamental assumptions of molecular chaos and binary interaction do not always apply and must be addressed.

Recent research [20,32] has concentrated on refining the molecular chaos assumption to account for velocity correlations in the dilute regime, which have been measured extensively [31,33–36]. However, in the dense regime, where networks of interacting grains become important, even an exact inclusion of velocity correlations will not accurately describe the physics since the binary collision assumption does not apply. In this regime it is important to take into account elastic stresses that arise from long-lasting interactions between grains, in addition to the collisional stresses that kinetic theory considers. In the next section we introduce a model to incorporate the elastic stress.

III. DENSE INERTIAL FLOWS

Dense inertial flows are not quasistatic and cannot be modeled by assuming binary interactions between grains. Long-lived contacts arise in this regime, which result in force networks that contain many grains, but do not span the shearing volume [2]. Dense inertial flows occur in the range of densities between the dilute and quasistatic regimes and exhibit properties of both limits. Like dilute flows, dense inertial flows are characterized by a Bagnold rheology where the stress tensor is proportional to the square of the shear rate [37–40]. However, as in quasistatic flows, the value of the stress tensor also depends on the properties of force chain networks which grow to sizes $\xi \gg 1$.

An ideal constitutive model of granular shear flow would enable a full determination of the stress tensor in all regimes of granular flow. While most models are specialized to either the dilute or quasistatic regimes, there is evidence that a model based on the inertial number, a dimensionless number proportional to the shear rate divided by the square root of pressure, would enable a description that spans all densities, including the dense inertial flows [38,40]. Low values of the inertial number would correspond to quasistatic flows, high values to dilute flows, and intermediate values to dense inertial flows.

Here we focus on the properties of force networks in constructing a constitutive model for granular shear flow at all densities. The central concept of our model is that forces are transferred elastically through finite-sized contact networks and the value of the contact force between any pair of grains depends on both the relative velocity of the contacting pair (a "collisional" contribution inspired by kinetic theory) and the values of the other contact forces in the network, even those a long distance away (an "elastic" contribution). This leads to predictions for all components of the stress tensor, which are shown to hold over the entire inertial regime without fitting parameters, and incorporate the noncollisional stress that arises when force networks have formed. While the resulting expressions are somewhat complex, the central concept of forces propagating through networks is basic and fundamental. Since the model accurately predicts the stress tensor, it also predicts the inertial number and yields simple scaling relationships near jamming at ν_c and the network transition at ν_{bc}.

An important parameter that emerges from this analysis is the network size ξ. Like the inertial number, ξ is a parameter that is relevant in all regimes of granular flow. It varies continuously from the dilute regime, where interactions are binary and the network size is unity, to the quasistatic regime where force chain networks extend over the entire system. Since our model predicts the inertial number as a function of ξ, this raises the possibility that other observables in granular flow can be described in terms of network parameters and a mesoscopic length scale is underlying much of the complex behavior seen in granular flow.

A. Force network model

An important feature of dense granular materials is that forces can be transferred over distances much larger than the grain size. This is especially evident in static packings of grains, but is also important when considering dense flows. The only necessary requirement for spatial force propagation is the existence of connected networks of interacting grains. When this requirement is met, elastic waves propagate through the networks at a speed set by the values of the elastic moduli and there is an elastic component of the stress tensor. This elastic contribution must be added to the collisional part of the stress in Eq. (5) to yield the full static stress tensor of Eq. (2). Therefore the full static stress tensor is comprised of two components: one describing the elastic response and one describing the collisional response.

From a microscopic viewpoint, the value of the static stress tensor is determined by contact forces between grains, as in Eq. (2). Therefore, in the presence of force networks, these contact forces must also be comprised of collisional and elastic components. The collisional component is given by Eq. (4) and represents the local force due to collisions between pairs of grains. It depends only on properties of the two contacting grains. The elastic component is a result of elastic deformations in the contact network. It is a nonlocal force that arises from the network applying an effective pressure on every pair of contacting grains.

In dilute flows only the collisional component of contact forces is nonzero and the static stress tensor is well described by kinetic theory. In the quasistatic regime the elastic component of the forces is much larger than the collisional component and the latter is usually disregarded. In dense inertial flows, both components contribute. The force network model extends hard-sphere kinetic theory by explicitly calculating the effects of elastic waves in force networks. This leads to a prediction for the elastic component of contact forces, which result from forces propagating through force networks at the elastic wave speed. Inertial flows correspond to the limit where forces propagate throughout the entire network before it is destroyed, which ensures that the shear rate remains the only relevant time scale. This is equivalent to the limit where the elastic wave speed is infinite, or the grains are perfectly rigid. It is the limit we address here.

Mathematically, the contact force F^{ij} between grains i and j is equal to the sum of a collisional term plus elastic effects from the network:

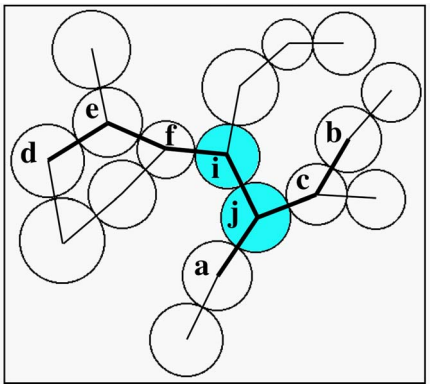

FIG. 3. (Color online) A typical force network of grains from simulations with $e=0$ and $\nu=0.75$. Grains not connected to this particular cluster are not shown. In the force network model, the elastic force between grains i and j arises from collisional forces that propagate through the network. Lines are drawn between contacting grains, with the bold lines illustrating different paths through the network. The path $d\rightarrow e\rightarrow f\rightarrow i$ is defined as a path of length $\ell=3$ since the collisional force F_{bc}^{de} must travel through three grains to affect the contact $\{i,j\}$. Also illustrated are paths of length $\ell=1$ $(a\rightarrow j)$ and $\ell=2$ $(b\rightarrow c\rightarrow j)$. At each link in a path, the transferred force is reduced by a factor equal to the cosine of the angle made by the lines. The total elastic force is determined by summing over all possible paths through the network.

$$F^{ij}=F_{\mathrm{bc}}^{ij}+\sum_{\ell=1}^{\ell_{\max}}\mathcal{F}_{\ell}^{ij}. \tag{16}$$

In this equation the first term is the collisional force, defined in Eq. (4), and the second term arises from forces that propagate through paths in the force chain network, as illustrated in Fig. 3. We find it convenient to split this term into contributions $\mathcal{F}_{\ell}^{ij}$ that represent added forces from different path lengths ℓ. The total elastic force created by the network is then equal to the sum of the contributions $\mathcal{F}_{\ell}^{ij}$ over all possible path lengths $\ell<\ell_{\max}$ that elastic waves propagate through the force network.

Figure 3 illustrates force propagation and defines the notion of path length on a network topology. For example, a collision between grains d and e increases the force between grains e and f, which increases the force between grains f and i, which has the net effect of increasing the contact force between grains i and j. We denote this as a path of length 3 $(\ell=3)$ since the local force F_{bc}^{de} must propagate through three links to influence the contact between i and j. Paths of length $\ell=2$ and $\ell=1$ are also illustrated.

Given the topology of the network and the collisional forces on all contacts, our aim is to determine the value of the resulting elastic forces. In the limit of rigid grains, where grain stiffnesses are infinite, two important simplifications can be applied. First, infinite stiffness implies infinite wave speed, and therefore forces propagate instantaneously. This means that the time it takes for forces to propagate through a network is much smaller than the network lifetime and the network topologies can be considered static. Second, forces are not related to grain deformations (or overlaps) and therefore energy is only dissipated in collisions. This implies that no energy is lost as forces propagate through a network. For soft grains with finite stiffness, these two simplifications do not apply: the network topology changes as forces propagate and additional energy is dissipated in the process.

While soft grains more closely resemble experimental systems, the rheologies of soft and rigid grains are identical (and inertial) if the stiffness of the soft grains is above a threshold [41]. By investigating properties of rigid grains we can predict the stress tensor in inertial granular flows. In this limit, due to constraints from the network, interacting grains cannot properly recoil from a collision event and the initial kinetic energy that would have been transformed into grain velocities is instead transformed into elastic potential energy of the network. The transfer of energy leads to elastic forces and is quantified below.

We begin by considering a path of length $\ell=1$, as illustrated in Fig. 3. Because grain a is in contact with grain j, the local contact force F_{bc}^{ja} increases the value of F^{ij} by some amount. The magnitude of the increase can be determined by the following argument: if grain j had no contacts other than a, the collisional force F_{bc}^{ja} would result in a velocity of grain j with magnitude proportional to F_{bc}^{ja} and in the direction of the unit vector between grains a and j, denoted here as $\hat{\boldsymbol{\sigma}}^{ja}$. However, since j is in contact with i, the velocity that would have been created in the direction of $\hat{\boldsymbol{\sigma}}^{ij}$ is instead transformed into elastic potential energy and thereby a force between grains i and j. In accordance with Eq. (4), the magnitude of the transferred force is proportional to the velocity of grain j in the direction of $\hat{\boldsymbol{\sigma}}^{ij}$, which is in turn proportional to the collisional force F_{bc}^{ja} multiplied by the cosine of the angle between the unit vectors connecting contacts $\{a,j\}$ and $\{i,j\}$. This yields a extra contact force of $\hat{\boldsymbol{\sigma}}^{ij}\cdot\hat{\boldsymbol{\sigma}}^{ja}F_{\mathrm{bc}}^{ja}$ at the contact $\{i,j\}$, due to the collision between $\{a,j\}$. Note that we have implicitly assumed that the kinetic energy is transformed into elastic potential energy *without any dissipation*. This is a consequence of the rigid grain limit, where particles are either in contact with zero relative velocity or out of contact. In this limit, energy is only dissipated upon collisions and no energy is dissipated as forces propagate through networks. Paths of length $\ell=1$ are the simplest case of force transfer, and we have verified in contact dynamics simulations of three grains that forces are indeed reduced by the cosine of the angle.

More generally, if grain i has z_i contacts labeled by m and grain j has z_j contacts labeled by n, then the effect of all paths of length 1 is to increase F^{ij} in Eq. (16) by an amount

$$\mathcal{F}_{1}^{ij}=\sum_{m=1;m\neq j}^{z_i}\hat{\boldsymbol{\sigma}}^{ji}\cdot\hat{\boldsymbol{\sigma}}^{jm}F_{\mathrm{bc}}^{im}+\sum_{n=1;n\neq i}^{z_j}\hat{\boldsymbol{\sigma}}^{ij}\cdot\hat{\boldsymbol{\sigma}}^{jn}F_{\mathrm{bc}}^{jn}, \tag{17}$$

where $\hat{\boldsymbol{\sigma}}^{ab}$ is the unit vector connecting the center of grains a and b. This expression includes all of the effects from paths of length $\ell=1$ on each of the contacting grains i and j. To better understand the origin of the expression in Eq. (17), it is useful to read the terms in the summations from right to left. In particular, for the first term, the collisional force F_{bc}^{im} increases the force on contact $\{i,j\}$ by an amount given by the cosine of the angle in the path $\hat{\boldsymbol{\sigma}}^{ji}\cdot\hat{\boldsymbol{\sigma}}^{im}$. Similarly, for the

second term, the collisional force F_{bc}^{jn} increases the force on contact $\{i,j\}$ by a similar cosine $\hat{\boldsymbol{\sigma}}^{ij}\cdot\hat{\boldsymbol{\sigma}}^{jn}$.

In an analogous manner, we can also determine the effect of paths of length 2. The path from grain b to c to j in Fig. 3 comprises a path of length 2 ($\ell=2$), which increases the value of F^{ij} due to the local force between b and c. Note that we ignore the fact that the local force between c and j also increases F^{ij}, since this contribution was already included in the $\ell=1$ expression of Eq. (17). The total additional force between grains i and j arising from paths of length 2 is given by

$$\mathcal{F}_2^{ij} = \sum_{m=1;m\neq j}^{z_i} \hat{\boldsymbol{\sigma}}^{ji}\cdot\hat{\boldsymbol{\sigma}}^{im} \sum_{p=1;p\neq m}^{z_m} \hat{\boldsymbol{\sigma}}^{im}\cdot\hat{\boldsymbol{\sigma}}^{mp}F_{\mathrm{bc}}^{mp} + \sum_{n=1;n\neq i}^{z_j} \hat{\boldsymbol{\sigma}}^{ij}\cdot\hat{\boldsymbol{\sigma}}^{jn} \sum_{q=1;q\neq n}^{z_n} \hat{\boldsymbol{\sigma}}^{jn}\cdot\hat{\boldsymbol{\sigma}}^{nq}F_{\mathrm{bc}}^{nq}, \tag{18}$$

where grain i has z_i contacts labeled by m and grain j has z_j contacts labeled by n. To calculate the effect of paths of length 2, we also take into account the z_m contacts of grain m, labeled by p, and the z_n contacts of grain n, labeled by q. Once again, it is useful to read these expressions from right to left. For the first term, the collisional force F_{bc}^{mp} is propagated to its nearest-neighbor contact $\{m,i\}$ and reduced by a factor of the cosine of the angle $\hat{\boldsymbol{\sigma}}^{im}\cdot\hat{\boldsymbol{\sigma}}^{mp}$. Then, the remaining portion of the original collisional force is again propagated to the contact of interest $\{i,j\}$ and further reduced by the cosine of the angle $\hat{\boldsymbol{\sigma}}^{ji}\cdot\hat{\boldsymbol{\sigma}}^{im}$. So paths of length 2 correspond to force propagation through contacts of contacts of grains i and j. At each link of the path the magnitude of the propagated force is decreased by the cosine of the angle between subsequent contacts.

The contributions to F^{ij} from path length $\ell>2$ can be determined by continuing the above arguments. They depend on the coordination number z and are also sensitive to the geometric arrangement of force networks. For example, to incorporate paths of length 3 we would need to include contacts of contacts of contacts. The sums would contain terms of the form

$$(\hat{\boldsymbol{\sigma}}^{ji}\cdot\hat{\boldsymbol{\sigma}}^{im})(\hat{\boldsymbol{\sigma}}^{im}\cdot\hat{\boldsymbol{\sigma}}^{mn})(\hat{\boldsymbol{\sigma}}^{mn}\cdot\hat{\boldsymbol{\sigma}}^{no})F_{\mathrm{bc}}^{no} \tag{19}$$

summed over grains m, n, and o, which are contacts of grains i, m, and n, respectively. This expression includes three cosine factors (one for each link in the path) and one collisional force at the end of the path, which corresponds to the distant collisional force having a progressively weaker effect as it propagates through many links in the network. Similar expressions can be written for arbitrary path lengths.

One important constraint arises as z becomes large, which is a result of energy conservation. If we consider the total energy T^{ij} that an arbitrary contact $\{i,j\}$ transfers to the network, this must always be less than or equal to the total kinetic energy initially stored in the contact (via the kinetic energies of grains i and j). This is because, while energy must be conserved in this process, some is transferred to the elastic energy of the network and some remains as kinetic energy of grains i and j. The average collisional force $\langle F_{\mathrm{bc}}^{ij}\rangle$ is proportional to the square of the relative velocities [15] and thereby proportional to the kinetic energy contained in the contact. Therefore, on average, the *magnitude* of the collisional force transferred to nearest neighbors must not be greater than $\langle F_{\mathrm{bc}}^{ij}\rangle$.

The total force transmitted from contact $\{i,j\}$ to its nearest neighbors is given by

$$\sum_{m=1;m\neq j}^{z_i} \hat{\boldsymbol{\sigma}}^{mi}\cdot\hat{\boldsymbol{\sigma}}^{ij}F_{\mathrm{bc}}^{ij} + \sum_{n=1;n\neq i}^{z_j} \hat{\boldsymbol{\sigma}}^{nj}\cdot\hat{\boldsymbol{\sigma}}^{ji}F_{\mathrm{bc}}^{ji}. \tag{20}$$

Due to the fact that energy is conserved, the sum of Eq. (20) over every contact must be less than the sum collisional force over every contact. Therefore, on average for each contact, we have that

$$T^{ij} \equiv \left\langle \left(\sum_{m=1;m\neq j}^{z_i} \hat{\boldsymbol{\sigma}}^{mi}\cdot\hat{\boldsymbol{\sigma}}^{ij}F_{\mathrm{bc}}^{ij} + \sum_{n=1;n\neq i}^{z_j} \hat{\boldsymbol{\sigma}}^{nj}\cdot\hat{\boldsymbol{\sigma}}^{ij}F_{\mathrm{bc}}^{ij} \right) \right\rangle \leq \langle F_{\mathrm{bc}}^{ij}\rangle, \tag{21}$$

which is a global constraint. It ensures that the total energy supplied to the network never exceeds the initial kinetic energy as the elastic waves move from first-nearest neighbors, to second-nearest neighbors, and so on.

Equations (17)–(21) model the physical origin of elastic forces that exist in dense granular materials and allow for a complete determination of $\mathcal{F}_\ell^{ij}$. The numerical value of the elastic force between a pair of contacting grains is calculated by summing these contributions over all possible path lengths ℓ, as in Eq. (16).

The maximum possible path length $\ell_{\max}$ is constrained by the size of the force networks. A straight chain of grains that spans the network has $\ell^*=\xi/\xi_{\mathrm{el}}-1$. While there are also network spanning chains with $\ell>\ell^*$, their contributions to elastic forces are diminished since the magnitude of the collisional force at the end of the chain is reduced by the product of the cosine of the angles in the chain. We will therefore set $\ell_{\max}=\xi/\xi_{\mathrm{el}}-1$ and only consider the network spanning chains that give the largest contribution. This amounts to completely ignoring the effects of path lengths with $\ell>\ell_{\max}$ which increase the elastic force on the contact $\{i,j\}$ by an amount $\Delta=\Sigma_{\ell=\ell_{\max}+1}^{\infty}\mathcal{F}_\ell^{ij}$. We do not expect this approximation to produce a large error in the total elastic force on $\{i,j\}$ since $\Delta<\mathcal{F}_{\ell_{\max}}^{ij}$ and, in general, $\mathcal{F}_{\ell+1}^{ij}\ll\mathcal{F}_\ell^{ij}$ for $\ell<\ell_{\max}$.

Given the above analysis, it is possible to completely determine the stress tensor based on properties of the force network and the collisional stresses. This is carried out in Sec. III B and the predictions are tested in Sec. III C.

B. Calculating the stress tensor

The analysis in the previous section holds in any spatial dimension. However, in order to predict the stress tensor, we find it necessary to rewrite the equations of the force network model in terms of integrals instead of sums. Here we carry out this substitution for a two-dimensional system, although it can be generalized to higher dimensions, resulting in slightly more complex equations.

If we consider the average force between two grains that contact at an angle θ, denoted $F(\theta)$, then Eq. (16) can be generalized to read

$$F(\theta) = F_{\mathrm{bc}}(\theta) + \sum_{\ell=1}^{\xi/\xi_{\mathrm{el}}-1} \mathcal{F}_\ell(\theta). \tag{22}$$

This equates the average force between grains contacting at angle θ to the average collisional force at that angle, plus elastic effects from the network. In what follows we will measure θ with respect to the axis of shear, so that $\theta=0$ corresponds to the axis where there is no gradient in grain velocities.

Generalizing Eqs. (17) and (18) to arbitrary path length ℓ gives

$$\mathcal{F}_\ell(\theta_0) = \prod_{i=1}^{\ell} (z-1) \int_{\theta_{i-1}-2\pi/3}^{\theta_{i-1}+2\pi/3} d\theta_i \cos(\theta_i - \theta_{i-1}) \times P_C(\theta_i - \theta_{i-1}) C(\theta_i) F_{\mathrm{bc}}(\theta_\ell). \tag{23}$$

In this equation, the sums from Eqs. (17) and (18) have been replaced by integrals over θ_i, which is the angular orientation of each link in the chain. Each integral contains a cosine that replaces the dot product. Note that the bounds of the integrals are arranged such that the grain at link i is not permitted to overlap the grain at link $i-1$. The function $F_{\mathrm{bc}}(\theta_\ell)$ provides the collisional force at the end of the path. In order to properly characterize the probability to have a contact at θ_i, we also introduce the functions $C(\theta)$ and P_C. $C(\theta)$ gives the probability to have a single contact at angle θ [42–46]. In the case that there are two (or more) contacts on a single grain, which is necessary to form a chain, this probability must be modified [47]. The function $C(\theta_i)P_C(\theta_i-\theta_{i-1})$ gives the conditional probability to have a contact at θ_i, provided that there is already a contact at θ_{i-1}. P_C depends on the average number of contacts, z, and the averaged fluctuations of z in a given network. The prefactor $z-1$ gives the average number of contacts to which the collisional force is transferred.

Equation (23) generalizes the sums in Eqs. (17) and (18) to arbitrary path length ℓ. It does so by averaging over one-particle distribution functions. These come in the form of the average collisional force $F_{\mathrm{bc}}(\theta)$, the average contact probability on a single grain $C(\theta_i)P_C(\theta_i-\theta_{i-1})$, and the average coordination number z. Naturally, there must not be correlations between these variables in order for the predictions to apply. The definition of P_C ensures that there are no correlations between the contact probabilities and the coordination number, but it is not guaranteed that the collisional forces are not correlated with the network structure. In fact, when closed loops form in the force networks, the collisional forces and network structure do become correlated. Therefore, Eq. (23) only applies as a mean-field approximation that ignores the correlations induced from loops in the force networks. This is a valid approximation since the effect of a collisional force that propagates around a loop is reduced by the product of the cosine of the angles around the loop, which is quite small compared with direct propagation.

To solve the integrals in Eq. (23), we change integration variables to $x_i=\theta_i-\theta_{i-1}$. This results in the expression

$$\mathcal{F}_\ell(\theta) = \prod_{i=1}^{\ell} (z-1) \int_{-2\pi/3}^{2\pi/3} dx_i \cos(x_i) P(x_i) \times C\left[\theta + \sum_{j=1}^{i} x_j\right] F_{\mathrm{bc}}\left[\theta + \sum_{j=1}^{\ell} x_j\right], \tag{24}$$

which incorporates the average effect of all forces that propagate through paths of length ℓ on contacts with orientation θ.

In addition to force propagation based on the cosine of the angle between subsequent contacts, we must also incorporate the global constraint from Eq. (21). This can be generalized to

$$T(\theta) = \langle F_{\mathrm{bc}}(\theta)\rangle (z-1) \int_{-2\pi/3}^{2\pi/3} dx P_C(x) \cos(x) C(\theta + x) \leq \langle F_{\mathrm{bc}}(\theta)\rangle \tag{25}$$

and restricts the total energy transferred through the network.

Equations (24) and (25), combined with the basic force network Eq. (22), comprise the integral form of the force network model. In order to carry out the integrations, it is necessary to know the functional form of $C(\theta)$ and $F_{\mathrm{bc}}(\theta)$. These functions are π periodic and can be written as a Fourier series, keeping only terms that are also π periodic. Previous research on the contact probability [42–46] has shown that $C(\theta)$ is well approximated by keeping only the lowest Fourier terms. We find that $F_{\mathrm{bc}}(\theta)$ has the same property. We therefore approximate

$$C(\theta) = \frac{1}{2\pi}(1 + a_c \sin 2\theta + a_c' \cos 2\theta), \tag{26}$$

$$F_{\mathrm{bc}}(\theta) = \langle F_{\mathrm{bc}}\rangle (1 + a_f \sin 2\theta + a_f' \cos 2\theta). \tag{27}$$

In Fig. 4 we plot data of these functions for a granular material with $e=0$ and $\nu=0.79$, along with a fit to the above equations. The fit is constructed by computing the fabric tensor $\phi_{\alpha\beta}=\langle \hat{\sigma}_\alpha \hat{\sigma}_\beta \rangle$ and force-fabric tensor $\chi^{(n)}_{\alpha\beta} = \langle F_{\mathrm{bc}} \hat{\sigma}_\alpha \hat{\sigma}_\beta \rangle / \langle F_{\mathrm{bc}} \rangle$, where $\hat{\sigma}_\alpha$ is the α component of the unit vector between contacting grain centers, F_{bc} is the collisional force on the contact, and the average is taken over all contacts. The anisotropies in the contact and force distributions $\{a_c, a_c', a_f, a_f'\}$ are related to eigenvalues of the fabric tensors [45], which are simple to measure. We see from the plots that this first-order approximation for the contact probability and collisional force is quite good.

We have measured $C(\theta)$ and $F_{\mathrm{bc}}(\theta)$ for a wide range of restitution coefficients and packing fractions. In Fig. 5 we plot the value of the Fourier components from Eqs. (26) and (27), which characterize the functional form in all cases. These plots reveal that the anisotropy in both the contact probability and collisional force depends sensitively on the value of the packing fraction and restitution coefficient. The size of the components is of the order of 10^{-1} whereas the magnitude of the next-order coefficients in the Fourier series

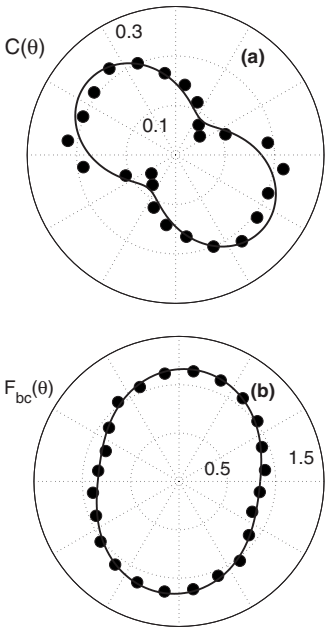

FIG. 4. Polar plots of measurements (data points) and fits (lines) of (a) the contact probability distribution $C(\theta)$ and (b) the collisional force distribution $F_{\rm bc}(\theta)/\langle F_{\rm bc}\rangle$ for a granular material with $e=0$ and $\nu=0.79$. The lines are fits of Eqs. (26) and (27), and the values of the Fourier components are plotted in Fig. 5.

is much smaller. This allows us to truncate the series in Eqs. (26) and (27) at first order and still get good agreement with the actual data, as in Fig. 4.

Now that we have a functional form for $C(\theta)$ and $F_{\rm bc}(\theta)$, we can solve for $\mathcal{F}_\ell(\theta)$ to first order in the Fourier components $\{a_c,a_c',a_f,a_f'\}$. This gives

$$\mathcal{F}_\ell(\theta)=\langle F_{\rm bc}\rangle(z-1)^\ell(\Phi^\ell+\Psi^\ell(a_f\sin 2\theta+a_f'\cos 2\theta)+\sum_{i=1}^{\ell}\Psi^i\Phi^{\ell-i}(a_c\sin\ 2\theta+a_c'\cos 2\theta)), \tag{28}$$

where Φ and Ψ are variables that depend on the geometry of the force networks and are expressible as

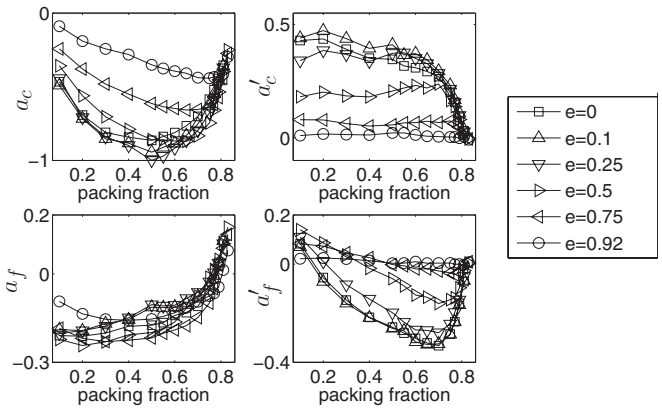

FIG. 5. Measured values of the Fourier components from Eq. (27).

$$\{\Phi,\Psi\}=\int_{-2\pi/3}^{2\pi/3}dxP_C(x)\cos(x)\{1,\cos(2x)\}. \tag{29}$$

We can also solve for the constraint in Eq. (25). To lowest order in the Fourier components, the constraint equation gives

$$\frac{T(\theta)}{\langle F_{\rm bc}(\theta)\rangle}=\Phi(z-1)\le 1. \tag{30}$$

This, combined with Eq. (28), provides a closed formula for $\mathcal{F}_\ell$:

$$\mathcal{F}_\ell(\theta)=\langle F_{\rm bc}\rangle\Big(\min[\Phi(z-1),1]^\ell+\Psi^\ell(z-1)^\ell\times(a_f\sin 2\theta+a_f'\cos 2\theta) \tag{31}$$

$$+\sum_{i=1}^{\ell}\Psi^i(z-1)^i\min[\Phi(z-1),1]^{\ell-i}\times(a_c\sin 2\theta+a_c'\cos 2\theta)\Big), \tag{32}$$

to first order in $\{a_c,a_c',a_f,a_f'\}$, where $\min[A,B]$ is equal to the smaller of A and B.

This solution can now be used to arrive at a constitutive relation for the stress tensor. The static stress tensor is given by Eq. (2), which can be rewritten in two dimensions as

$$\Sigma^{\rm s}_{\alpha\beta}=\frac{1}{V}\int d\theta C(\theta)\sigma(\theta)F(\theta)\begin{pmatrix}\cos^2\theta & \cos\theta\sin\theta\\ \cos\theta\sin\theta & \sin^2\theta\end{pmatrix}, \tag{33}$$

where $\sigma(\theta)$ is the average value of the distance between grains at contact for a given angle. In our simulations we observe that $\sigma(\theta)$ has very little dependence on θ (of the order of less than 10^{-4}). Thus $\sigma(\theta)=\langle\sigma\rangle$. We can also use this same integral form to determine the collisional stress tensor by replacing $F(\theta)$ with $F_{\rm bc}(\theta)$.

In this paper we have concentrated on the pressure and shear stress. The pressure is given by one-half the trace of Eq. (33) and the shear stress by either off-diagonal element, but these two quantities do not fully describe the stress tensor. There is a third independent term and, without loss of generality, we use Σ_{11}. Inserting the solution for $F(\theta)$ from Eqs. (22) and (32) into Eq. (33), we arrive at the following constitutive relations that fully describe the stress tensor:

$$\frac{p^{\rm s}-p^{\rm bc}}{p^{\rm bc}}=\sum_{\ell=1}^{\xi/\xi_{\rm el}-1}\min[\Phi(z-1),1]^\ell, \tag{34}$$

$$\frac{s^{\rm s}-s^{\rm bc}}{p^{\rm bc}}=\frac{1}{2}\sum_{\ell=1}^{\xi/\xi_{\rm el}-1}\Big(a_f\Psi^\ell(z-1)^\ell+a_c\sum_{i=0}^{\ell}\Psi^i(z-1)^i\times\min[\Phi(z-1),1]^{\ell-i}\Big), \tag{35}$$

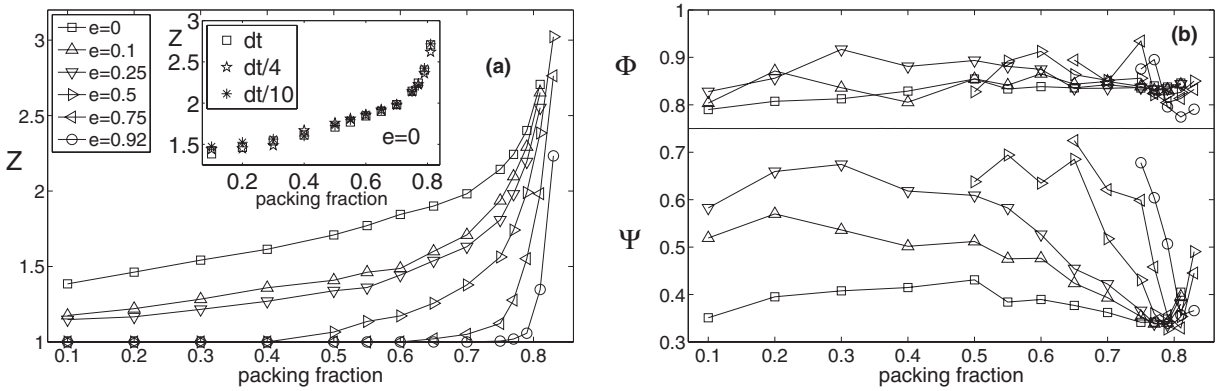

FIG. 6. (a) The coordination number z and (b) Φ and Ψ [Eq. (29)] for a wide variety of packing fractions and restitution coefficients. The line labels (e values) in (b) are the same as in (a). Although z and Ψ depend sensitively on the value of ν and e, the value of Φ is always approximately 0.83.

$$\frac{\Sigma_{11}^{s}-\Sigma_{11}^{bc}}{p^{bc}}=\sum_{\ell=1}^{\xi/\xi_{el}-1}\left(\min[\Phi(z-1),1]^{\ell}+\frac{a_f'}{2}\Psi^{\ell}(z-1)^{\ell}+\frac{a_c'}{2}\sum_{i=0}^{\ell}\Psi^{i}(z-1)^{i}\min[\Phi(z-1),1]^{\ell-i}\right). \quad (36)$$

These equations relate the static stress tensor to its collisional values and properties of the force networks. The left-hand side (lhs) of each equation gives the difference between the static and collisional values of stress, which is equivalent to the elastic stress components. These differences are equal to network properties on the rhs of each equation, which are summed over all possible force chain path lengths ℓ in the network. The relevant network parameters are the network size ξ/ξ_{el}, the average number of contacts per grain, z; the components $\{a_f,a_f'\}$, which give the angular dependence of the average contact force on a grain via Eq. (27); the components $\{a_c,a_c'\}$, which give the angular dependence of the number of contacts on a grain via Eq. (26); and $\{\Phi,\Psi\}$, which are geometrical variables related to the probability of having multiple contacts on a single grain, as defined in Eq. (29).

A large number of network parameters appear in the constitutive equations, which makes their form rather complicated. This is to be expected, since the structure of the force networks is complex and the predictions of Eqs. (34)–(36) span system behavior from very dilute granular materials with $\phi\approx 0$ to dense granular materials with ϕ arbitrarily close to ϕ_c (and for all restitution coefficients e). The properties of the networks change considerably over this range of parameter space, and they must be retained in the equations.

Simple scaling relations can be obtained near certain packing fractions. For example, near the network transition at ν_{bc}, Eqs. (34)–(36) predict that $(\Sigma_{\alpha\beta}^{s}-\Sigma_{\alpha\beta}^{bc})\propto(z-1)$. This is because, when $\xi/\xi_{el}\approx 1$ near ν_{bc}, the deviation from the collisional stress is dominated by forces transmitted between nearest neighbors. Therefore the excess number of contacts serves as the dominant scaling variable. In contrast, near the jamming transition at ν_c, networks are saturated so that Eq. (21) takes its maximum value and all of the kinetic energy from each contact is transferred to the network. In this case the stress tensor should depend on the size of the networks, and the constitutive relations indeed predict that $\Sigma_{\alpha\beta}^{s}\propto\xi$. This scaling is especially interesting since it suggests that the size of the networks is the important scaling variable, which might also control other features of the jamming transition. Indeed, once ξ becomes large, it is clusters of grains, and not individual grains, that serve as the basic thermodynamic degrees of freedom.

Finally, we consider the limit of $\xi/\xi_{el}\to 1$ where force networks consist of only two grains. In this limit the force network model predicts that $\Sigma_{\alpha\beta}^{s}=\Sigma_{\alpha\beta}^{bc}$, which is the appropriate result in the dilute regime where kinetic theory holds.

C. Testing the predictions

Equations (34)–(36) make predictions for all independent components of the stress tensor over the complete range of e and for $\phi<\phi_c$ and comprise the central result of the force network model. The difference between the static and collisional values of stress is related to features of the force networks. These include the anisotropies in the contact probability and collisional force $\{a_c,a_c',a_f,a_f'\}$, the size of the force networks ξ/ξ_{el}, the average coordination number z, and a pair of geometric variables $\{\Phi,\Psi\}$ that are defined in Eq. (29) and are related to the distribution of contacts on single grains. All of these variables except z, Φ, and Ψ have been measured previously in this paper or in Ref. [2]. Our next step is to measure z, Φ, and Ψ.

In Fig. 6 we plot the values of z, Φ, and Ψ as measured in our simulations. We measure z by averaging over long-lived contacts, which are pairs of contacting grains that were also contacting in the previous time step. This ensures that only the static backbone of the force network is considered and that transient contacts do not artificially increase the coordination number. This measurement does not depend on the time step, as shown in the inset. We also measure Φ and Ψ, as prescribed in Eq. (29), by averaging over the same set of contacts. We observe that $\Psi<\Phi$ for all granular materials we have considered.

We have now measured every variable in the constitutive relations of Eqs. (34)–(36). We can therefore test the validity

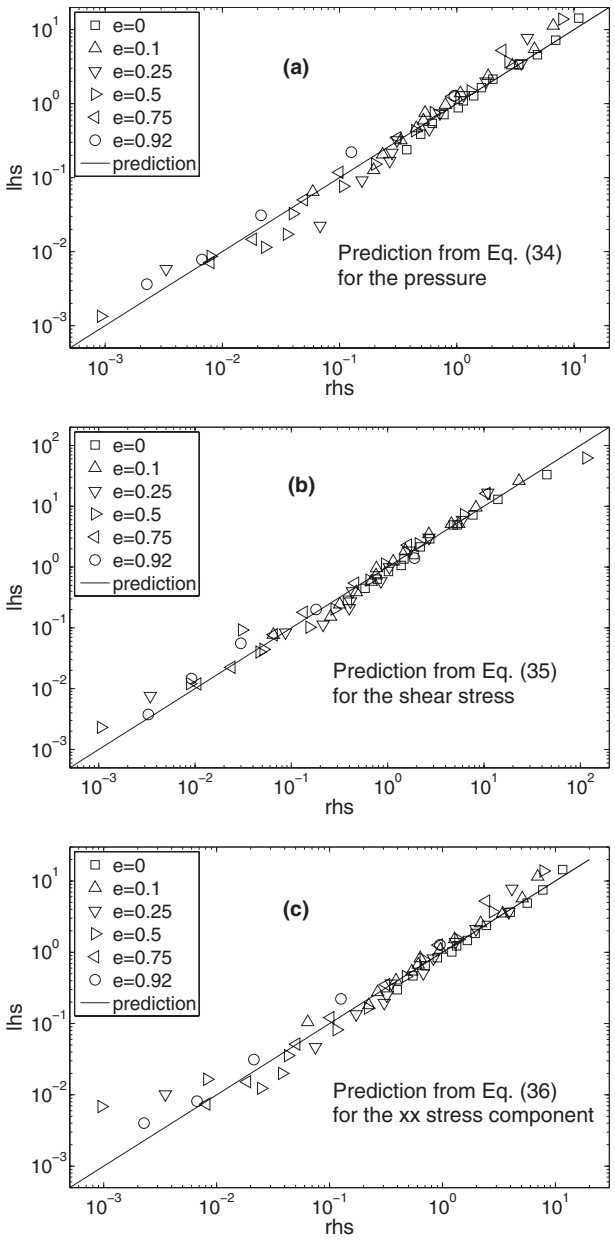

FIG. 7. Tests of the constitutive relations from the force network model. (a) Test of Eq. (34). The lhs of the equation, $\frac{p^s-p^{bc}}{p^{bc}}$, is plotted as a function of the rhs. This collapses the data to the line predicted by the model. (b) The lhs of Eq. (35), $\frac{s^s-s^{bc}}{p^{bc}}$, plotted as a function of the rhs, once again collapsing to the prediction. (c) The lhs of Eq. (36), $\frac{\Sigma_{11}^s-\Sigma_{11}^{bc}}{p^{bc}}$, plotted as a function of the rhs. All of the plots have been constructed using simulation data for each variable, and no fitting parameters have been utilized.

of the predictions without using any fitting parameters. Due to the complexity of the equations, it is convenient to plot the rhs of each equation versus the lhs. This is shown in Fig. 7 using all of the data we have collected. Plotted in this way, the data for each component of the stress tensor collapse onto the line predicted by the force network model over more than four decades. This collapse is especially striking since the variables in the predictions have a wide variance as a function of both restitution coefficient and packing fraction.

The collapse of our data onto the predicted curves suggests that the force network model captures an essential property of granular materials over a broad range of densities and restitution coefficients. The success of the model is based on visualizing granular materials as conglomerates of interacting networks, instead of collections of grains. Thus the packing fraction and restitution coefficient, which are grain properties, are substituted by the size, coordination, and other properties of the networks. This allows for constitutive relations to be determined analytically.

Finally, it is important to remark that the constitutive relations from the force network model have been derived in the limit of perfectly rigid grains, which may not always apply to realistic flows with finite grain stiffness. In the case of finite grain stiffness, there is a finite speed v_c at which forces propagate through the network. Combined with the lifetime of the networks τ_c, this sets a maximum correlation length $v_c\tau_c$, since information can only be transferred between a pair of grains if the network exists long enough to propagate it. This maximum correlation length is a monotonically increasing function of the grain stiffness. If $v_c\tau_c > \xi$, then the stress tensor can be described by Eqs. (34)–(36). However, if $v_c\tau_c < \xi$, it is necessary to replace the length scale ξ with $v_c\tau_c$. Because ξ diverges as the material approaches the jamming limit and $v_c\tau_c$ is always finite, we expect that for a given grain stiffness there is a critical packing above which $v_c\tau_c < \xi$. This critical packing fraction is always in the inertial regime and must be strictly less than ν_c. Therefore, very close to jamming, the elasticity of grains begins to play an important role. For all other packing fractions, the assumption of perfectly rigid grains is valid for natural and experimental flows.

IV. CONCLUSIONS

The underlying microscopic interactions between grains have a large influence on macroscopic characteristics of granular flow. We have investigated two models of the stress tensor—kinetic theory and the force network model—which make different assumptions about the microscopic interactions. Kinetic theory assumes that only binary collisions are relevant and calculates the stress tensor based on grain properties, whereas the force network model allows simultaneous interaction between many grains and calculates the stress tensor based on properties of the resultant force networks.

For dilute flows, which occur when the size of the force networks is small, kinetic theory makes accurate predictions. This is not surprising since small force networks imply localized interactions and binary collisions. For dense flows, force networks extend beyond pairs of grains and the predictions of kinetic theory no longer match data from simulations. This is because grain-grain correlations are induced via the force networks and kinetic theory does not take them into account. However, correlations never exist between isolated networks, and by constructing the force network model based on network properties, we are able to accurately predict the stress tensor for both dilute and dense flows.

The force network model predicts all independent components of the stress tensor over the entire inertial regime and

matches data from simulations for more than four decades. Extensions of the model could be used to predict other quantities, including the contact force distribution function $P(f)$. An integral part of any such theory is the finite size of the force networks, which has important effects on the qualitative features of $P(f)$ [2]. Further extensions could also specify relations between network parameters and thereby simplify the constitutive equations (34)–(36). While it is possible that the relations between network parameters are complicated and depend on many factors, it is likely that simple scalings exist near the network transition at ν_{bc}. For $\nu \approx \nu_{\mathrm{bc}}$ the deviation between the static and collisional stress tensors is proportional to $(z-1)$ and it is likely that network parameters also scale with powers of $(z-1)$. In particular, it would be interesting to probe the dependence of ξ on $(z-1)$, although fluctuations in the parameters have complicated our measurement of this relation.

Finally, while we have concentrated on the inertial regime, it is also important to understand how natural flows make the transition from dynamics dominated by inertia, to quasistatic dynamics, and ultimately to how the system jams. Along this sequence, the stiffness of the grains plays an increasingly active role in the dynamics. The force network model can accommodate the development of stiffness by incorporating a maximum length scale through which forces can propagate. Including this mechanism for a granular material moving through ν_c may help connect the dense inertial regime with the quasistatic regime and facilitate a more complete understanding of dry granular materials.

ACKNOWLEDGMENTS

This work was supported by the William M. Keck Foundation, the MRSEC program of the NSF under Grant No. DMR00-80034, the James S. McDonnell Foundation, the David and Lucile Packard Foundation, and NSF Grant Nos. DMR-9813752, PHY99-07949, and DMR-0606092.

[1] I. S. Aranson and L. S. Tsimring, Rev. Mod. Phys. **78**, 641 (2006).
[2] G. Lois, A. Lemaitre, and J. M. Carlson, preceding paper, Phys. Rev. E **76**, 021302 (2007).
[3] S. N. Coppersmith, C.-h. Liu, S. Majumdar, O. Narayan, and T. A. Witten, Phys. Rev. E **53**, 4673 (1996).
[4] J. E. S. Socolar, Phys. Rev. E **57**, 3204 (1998).
[5] P. Claudin, J.-P. Bouchaud, M. E. Cates, and J. P. Wittmer, Phys. Rev. E **57**, 4441 (1998).
[6] M. Nicodemi, Phys. Rev. Lett. **80**, 1340 (1998).
[7] J. E. S. Socolar, D. G. Schaeffer, and P. Claudin, Eur. Phys. J. E **7**, 353 (2002).
[8] M. Otto, J.-P. Bouchaud, P. Claudin, and J. E. S. Socolar, Phys. Rev. E **67**, 031302 (2003).
[9] J.-P. Bouchaud, P. Claudin, D. Levine, and M. Otto, Eur. Phys. J. E **4**, 451 (2001).
[10] S. Ogawa, in *Proceedings of the US–Japan Seminar on Continuum-Mechanical and Statistical Approaches in the Mechanics of Granular Materials*, edited by S. C. Cowin and M. Satake (Gakujutsu Bunker Fukyukai, Tokyo, 1978), pp. 208–217.
[11] P. K. Haff, J. Fluid Mech. **134**, 401 (1983).
[12] J. T. Jenkins and S. B. Savage, J. Fluid Mech. **130**, 187 (1983).
[13] C. K. K. Lun, S. B. Savage, D. J. Jeffrey, and N. Chepurniy, J. Fluid Mech. **140**, 223 (1984).
[14] J. T. Jenkins and M. W. Richman, Phys. Fluids **28**, 3485 (1985).
[15] V. Garzo and J. W. Dufty, Phys. Rev. E **59**, 5895 (1999).
[16] J. F. Lutsko, Phys. Rev. E **70**, 061101 (2004).
[17] J. F. Lutsko, Phys. Rev. E **72**, 021306 (2005).
[18] C. S. Campbell, Annu. Rev. Fluid Mech. **22**, 57 (1990).
[19] I. Goldhirsch, Annu. Rev. Fluid Mech. **35**, 267 (2003).
[20] T. P. C. van Noije and M. H. Ernst, *Kinetic Theory of Granular Gases*, in Vol. 564 of Lecture Notes in Physics, edited by T. Poschel and S. Luding (Springer-Verlag, Berlin, 2001).
[21] E. Azanza, F. Chevoir, and P. Moucheront, J. Fluid Mech. **400**, 199 (1999).
[22] D. Z. Zhang and R. M. Rauenzahn, J. Rheol. **44**, 1019 (2000).
[23] H. H. Shen and B. Sankaran, Phys. Rev. E **70**, 051308 (2004).
[24] D. Z. Zhang, Phys. Rev. E **71**, 041303 (2005).
[25] G. Lois, A. Lemaitre, and J. M. Carlson, Europhys. Lett. **76**, 318 (2006).
[26] G. Lois, A. Lemaitre, and J. M. Carlson, Comput. Math. (to be published).
[27] J. J. Brey, J. W. Dufty, and A. Santos, J. Stat. Phys. **87**, 1051 (1997).
[28] S. Chapman and T. G. Cowling, *The Mathematical Theory of Non-uniform Gases* (Cambridge University Press, Cambridge, England, 1970).
[29] J. H. Ferziger and H. G. Kaper, *Mathematical Theory of Transport Processes in Gases* (Elsevier, New York, 1972).
[30] S. Luding and A. Santos, J. Chem. Phys. **121**, 8458 (2004).
[31] S. J. Moon, M. D. Shattuck, and J. B. Swift, Phys. Rev. E **64**, 031303 (2001).
[32] T. P. C. van Noije and M. H. Ernst, arXiv:cond-mat/9706020.
[33] T. P. C. van Noije, M. H. Ernst, R. Brito, and J. A. G. Orza, Phys. Rev. Lett. **79**, 411 (1997).
[34] D. L. Blair and A. Kudrolli, Phys. Rev. E **64**, 050301(R) (2001).
[35] A. Prevost, D. A. Egolf, and J. S. Urbach, Phys. Rev. Lett. **89**, 084301 (2002).
[36] O. Pouliquen, Phys. Rev. Lett. **93**, 248001 (2004).
[37] L. E. Silbert, D. Ertas, G. S. Grest, T. C. Halsey, D. Levine, and S. J. Plimpton, Phys. Rev. E **64**, 051302 (2001).
[38] F. da Cruz, S. Emam, M. Prochnow, J.-N. Roux, and F. Chevoir, Phys. Rev. E **72**, 021309 (2005).
[39] G. Lois, A. Lemaitre, and J. M. Carlson, Phys. Rev. E **72**, 051303 (2005).
[40] GDR MIDI, Eur. Phys. J. E **14**, 341 (2004).
[41] W. R. Ketterhagen, J. S. Curtis, and C. R. Wassgren, Phys. Rev. E **71**, 061307 (2005).
[42] C. Thornton and D. J. Barnes, Acta Mech. **64**, 45 (1986).

[43] J. R. F. Arthur, J. A. Koenders, and R. K. S. Wong, Acta Mech. **64**, 19 (1986).
[44] L. Rothenburg and R. J. Bathurst, Geotechnique **39**, 601 (1989).
[45] F. Radjai, D. E. Wolf, M. Jean, and J.-J. Moreau, Phys. Rev. Lett. **80**, 61 (1998).
[46] N. P. Kruyt, Int. J. Solids Struct. **40**, 3537 (2003).
[47] H. Troadec, F. Radjai, S. Roux, and J. C. Charmet, Phys. Rev. E **66**, 041305 (2002).